Hydrodynamics of Superfluid Helium in a Single Nanohole

M. Savard, G. Dauphinais, and G. Gervais*

Department of Physics, McGill University, Montreal, Canada, H3A 2T8
(Received 15 June 2011; published 14 December 2011)

The flow of liquid helium through a single nanohole with radius smaller than 25 nm was studied. Mass flow was induced by applying a pressure difference of up to 1.4 bar across a 50 nm thick Si_3N_4 membrane and was measured directly by means of mass spectrometry. In liquid He I, we experimentally show that the fluid is not clamped by the short pipe with diameter-to-length ratio $D/L \simeq 1$, despite the small diameter of the nanohole. This viscous flow is quantitatively understood by making use of a model of flow in short pipes. In liquid He II, a two-fluid model for mass flow is used to extract the superfluid velocity in the nanohole for different pressure heads at temperatures close to the superfluid transition. These velocities compare well to existing data for the critical superflow of liquid helium in other confined systems.

Capillary flow experiments have been conducted for decades in micron sized channels but only recently has the technology become available to fabricate a cylindrical flow channel of any desired dimension in the nanometer range. Flow experiments across solid-state nanoholes (and nanopores) [1] have attracted a lot of attention over the past few years mainly for the detection of macromolecules [2]. The same fabrication technique can readily be used to study flow of many fluids, whether classical or quantum in nature. In this work, we are interested in the transport properties of a quantum fluid, liquid helium, flowing through a single cylindrical nanohole of 22.8 nm radius. This is motivated by a desire to understand the flow of liquid helium in very small apertures, where ultimately in the one-dimensional limit, the quantum fluid might form the long sought-after Luttinger liquid [3].

Liquid helium in constrained geometries behaves differently than in the bulk and has therefore been subject to extensive investigation in porous media such as Vycor [4], zeolites [5], and aerogel [6], as well as in superfluid films [7]. The experiment we present here has some advantages over these systems, which are made up of a large number of channels and the signal extracted from them is necessarily averaged over the whole distribution of dimensions and defects present in the material. The fabrication and detection method we use gives us complete control of the size and shape of the nanohole (from ∼1 nm to 100's of nm diameter), whereas porous media typically have fixed dimensions for a given material.

Confined systems have been of great interest for the study of superfluid helium, in particular, for the measurement of superfluid critical velocity. When superfluid helium is forced through a channel, it eventually reaches a critical velocity at which point it begins to dissipate energy, but exactly how a superfluid dissipates energy has been a long-standing problem in condensed matter physics. Critical velocities have been experimentally measured in many systems and were found to vary from mm/s to several m/s, values that are much lower than the Landau critical velocity, ∼60 m/s. This discrepancy and the strong dependence on channel diameter of observed critical velocities were explained by a size-dependent model of quantized vortices in the superfluid. Many other flow experiments found critical velocities independent of the system size and with a near-linear dependence on temperature [8]. These were coined intrinsic critical velocities so as to distinguish them from the "extrinsic" size-dependent ones and they have been studied by many groups [9–11] in superfluid flow experiments, for pores in the range of 10^{-5}–10^{-6} m. The currently accepted interpretation of these results is a thermally activated vortex nucleation process acting as a dissipation mechanism for the superfluid [12]. In this work, the superfluid flow constrained to a single nanometer-sized channel was studied such that its superfluid velocity could be inferred from the measured mass flow and compared with existing critical velocity data. To our knowledge this is the first time that a superfluid mass flow was directly detected for an aperture well in the nanometer scale regime.

Our sample is made from a 50 nm thick low-stress amorphous silicon nitride (Si_3N_4) layer grown on a 2.7 mm wide square silicon wafer with a region where the silicon was etched to obtain a rectangular silicon nitride membrane ∼30 μm wide. A cylindrical nanohole with 22.8 ± 0.7 nm radius was drilled in this membrane using a field emission TEM [see Fig. 1(a)]. Confirmation of the radius of the nanohole was accomplished by measuring the mass flow in the gas phase of helium at 20 K in the Knudsen regime. In this regime, a Knudsen effusion model of gas flow was shown previously [13] to give an accurate measure (within a few percent) of the nanohole radius. This gas flow measurement yielded a radius of 23.1 ± 0.5 nm for the sample used in this work. It was conducted after all data were taken and as such provides strong support that
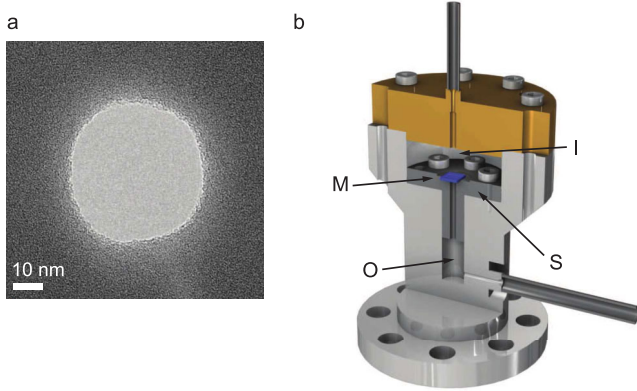
FIG. 1 (color). (a) TEM imaging of nanohole. (b) Schematics of the experimental cell. The SiN membrane (M) is epoxied to a support (S) to separate the cell between the inlet (I) and outlet (O).

the nanohole size remained unchanged throughout the experiment.

The sample wafer was epoxy sealed to a support made of Invar alloy separating two reservoirs (inlet and outlet) in an experimental cell designed such that any mass transfer between the two reservoirs is restricted to occur through the nanohole. Capillaries connect the extremities of the experimental cell to a gas handling system such that pressurized helium can be introduced in the cell, flow through the nanohole, and be pumped from the outlet of the cell by a mass spectrometer [see Fig. 1(b)]. We used silver powder packed heat exchangers to condense helium before it enters the inlet of the cell and to ensure a good thermal anchor to the cryostat. Since the outlet is kept under vacuum, the pressure P_{in} of the liquid helium above the membrane determines the pressure difference $\Delta P = P_{in} - P_{out} = P_{in}$ driving the mass flow through the nanohole. This mass flow was measured between 1.6 and 3.5 K and up to 1.4 bar of pressure difference across the nanohole. A calibrated leak of 4.5×10^{-3} ng/s $\pm 10\%$ was used to calibrate the mass spectrometer before the experiments.

A typical experiment goes as follows: we first empty both sides of the cell at a temperature well above the helium boiling point so as to ensure that no residual helium is present in either reservoir. The mass spectrometer is then connected to the outlet of the cell to determine a background signal that is treated as an offset to the pressure-driven flow of interest in this study. This background signal was always found to be below 5×10^{-4} ng/s, which is less than the mass flow measurement presented here by a few orders of magnitude. The next procedure is a cooling of the whole apparatus below the λ transition so that gaseous helium introduced from the gas handling system condenses and fills the heat exchanger and inlet of the experimental cell. Once condensation is achieved, the higher pressure above the membrane forces the liquid helium to flow through the nanohole. When atoms reach the very low

pressures in the lower reservoir, they evaporate and are pumped out to the mass spectrometer. The mass flow signal is then monitored as the temperature is slowly increased. This whole procedure was repeated at different pressure differences simply by varying the pressure P_{in} above the nanohole.

The results of several temperature sweeps are presented in Fig. 2. The mass flow was monitored at constant pressure while the temperature of the entire cell was increased from ~1.6 K to temperatures above T_λ. At each temperature, the system was given several minutes to equilibrate thermally until the mass flow signal reached a new constant value. The time constant for the system to converge to this new value was found to be between ~600 and ~1200 s, depending on temperature.

Focusing on the data at temperatures above T_λ in Fig. 2, our data unambiguously show a strong dependence of the mass flow on pressure. This means viscous flow of liquid helium through the nanohole is observed, and by extension that the flow of the normal component should not be ignored in helium II. Indeed one might naively make the assumption that it should be neglected since channels of the order of 10^{-7} m are frequently used as a superleak to clamp the normal component and measure exclusively superfluid signals. Our work shows this is not the case for this nanohole geometry.

Modeling of the mass flow must take into account the acceleration of the fluid at the ends of the short pipe, since the diameter-to-length ratio $D/L \simeq 1$ for this nanohole is too large for the infinite-pipe approximation to hold. A derivation for a viscous flow through a short cylindrical
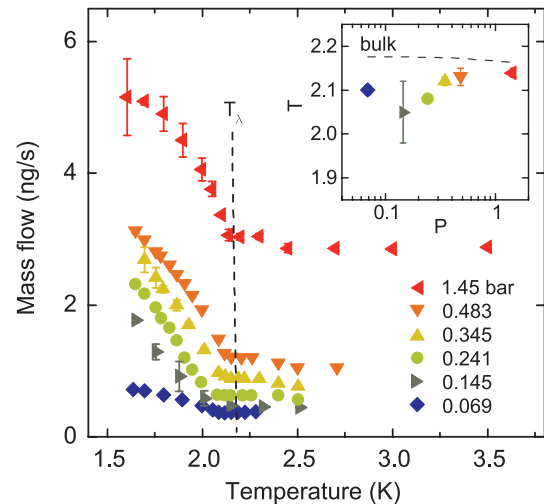

FIG. 2 (color). Mass flow of liquid helium in a single nanohole of 22.8 nm radius at pressure differences of 0.069, 0.145, 0.241, 0.345, 0.483, and 1.45 bar, respectively, from bottom to top. The inset shows the pressure dependence (in bar) of the transition temperature (in kelvin) for the onset of superfluid mass flow through the nanohole; the bulk superfluid transition T_λ is shown by a dashed line.

channel was derived by Langhaar [14] and gives $\Delta P = \frac{32\eta L v}{\rho D^2} + \frac{1}{2}\alpha v^2$, where α is a geometric parameter introduced to take into account the acceleration of the fluid near the ends, and η, ρ, and v are the dynamic viscosity, density, and average velocity, respectively. Solving for v gives

$$v = \frac{32\eta L}{\alpha\rho D^2}\left(\sqrt{1 + \frac{\alpha\rho D^4}{512\eta^2 L^2}\Delta P} - 1\right). \quad (1)$$

From the definition of mass flow $Q_m = \rho v A$, with A the effective area of the nanohole, we obtain

$$Q_m = \frac{8\pi\eta L}{\alpha}\left(\sqrt{1 + \frac{\alpha\rho R^4}{32\eta^2 L^2}\Delta P} - 1\right). \quad (2)$$

This mass flow equation can be fitted to the data in Fig. 2 (at temperatures above T_λ) using the radius R as a varying parameter. The strong dependence of Eq. (2) on the radius provides a quantitative test of our short-pipe model. In addition, the extracted radii can be readily compared to the TEM image taken before the measurements. The temperature and pressure dependence of η and ρ are known from the literature [15], and the length L of the short pipe was determined during the sample fabrication process. The value of the parameter $\alpha = 4.7$ was determined in earlier experiments on viscous gas flow in samples with very similar geometry [13]. The radii were extracted from all curves in Fig. 2, and the average radius is found to be $\bar{R} = 20$ nm with a standard deviation 2 nm. This value is in agreement with the radius of 22.8 ± 0.7 nm extracted from the TEM picture, giving us confidence in the appropriateness of the model used for the normal flow through the nanohole.

At temperatures below the λ transition, a strong increase in the mass flow is observed at all pressures. We attribute this increase in mass flow to the onset of the superfluid behavior in the nanohole. Indeed, as shown on Fig. 3 (green dotted line), the mass flow Q_m predicted by Eq. (2) using the tabulated total density of liquid helium and viscosity of the normal component is much smaller than what is experimentally observed; a superfluid contribution must therefore be included in the modeling of the flow. As presented in the inset of Fig. 2, this departure of the observed mass flow from the viscous flow prediction occurred at slightly lower temperature (T_λ^*) than the known superfluid transition (T_λ). While the exact nature of this small shift is unknown, it might be due to thermal or confinement effects in the nanohole. To account for this, we have used in the last two figures the temperature difference $T - T_\lambda^*$ rather than the absolute temperature (T) in order to compare more directly with past experiments.

The two-fluid model proposed by Tisza and Landau for flow density of He II is a natural starting point to model the flow when superfluid and normal helium participate in the

mass transport through the nanohole. In this model the total mass current is $\mathbf{J}_{\text{total}} = \rho_s\mathbf{v}_s + \rho_n\mathbf{v}_n$, where ρ_s and ρ_n are densities of superfluid and normal component of He II, respectively, and $\rho = \rho_s + \rho_n$. We consider the flow to be only in the axial direction of the nanohole so the total mass flow is given by $Q_m^{\text{total}} = J_{\text{total}}\pi R^2$. The normal part of He II can be described with the viscous short-pipe flow from above using the normal helium density in the equation. The total mass flow is therefore given by

$$Q_m^{\text{total}} = \pi R^2 \rho_s v_s + \frac{8\pi\eta L}{\alpha}\left(\sqrt{1 + \frac{\alpha\rho_n R^4}{32\eta^2 L^2}\Delta P} - 1\right). \quad (3)$$

We show in Fig. 3 (solid red line) the second term of Eq. (3) using the best radius to fit to the He I mass flow. The rapid drop of this term as temperature decreases indicates our measured signal is decreasingly caused by viscous normal flow. The normal component in the He II region was subtracted from the total flow measured to obtain the superfluid contribution to the mass flow. From this superfluid mass flow we can infer the average superfluid velocity using the first term on the right-hand side of Eq. (3). We have repeated this procedure for all data sets and have obtained the temperature dependence of the superfluid velocity in the nanohole. The critical velocities in other experiments are typically reached at pressure heads of $\sim O(1)$ Pa so given the larger pressure differences applied in our study, we assume the superfluid velocity measured must be critical as well and can be compared as such to existing data. In the inset of Fig. 4 we compare the superfluid velocities at 1.7 K to the critical velocities of many other experiments (taken from [16]). The open circles are identified as intrinsic critical velocities, whereas the cross
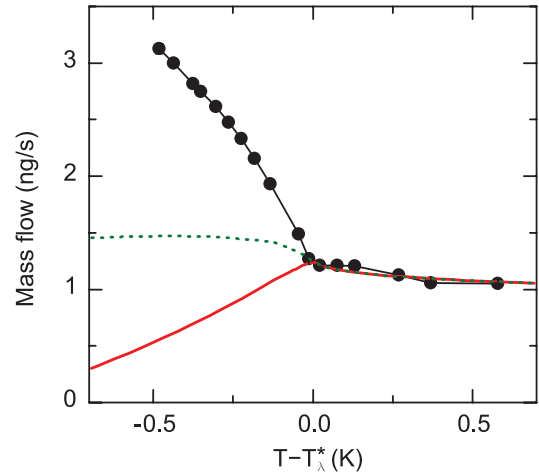

FIG. 3 (color). Mass flow measured at a pressure of 483 mbar (solid circle). The green dotted line shows the expected flow if only normal fluid flow was present (no superfluid component). The red curve [second term of Eq. (3)] is the viscous flow contribution in the two-fluid model for short pipe using the tabulated normal density. The black line is a guide to the eye.
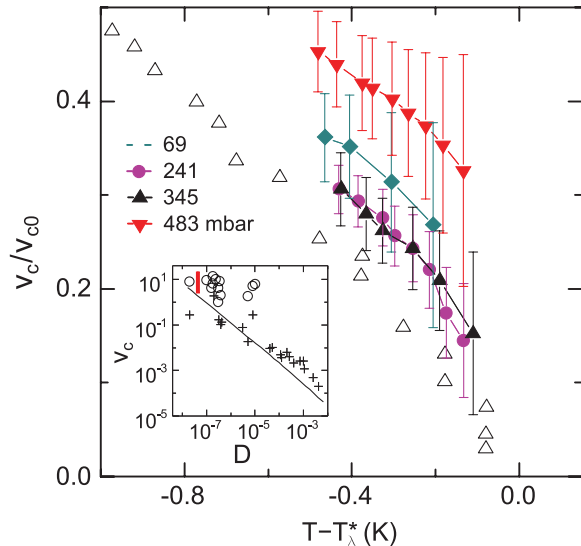
FIG. 4 (color). Temperature dependence of the normalized critical velocity. Open triangles (from [9]) are compared to our results (full symbols) at several pressures. (Inset) Critical velocity (in m/s) of superfluid helium from experiments in many different systems [16] as a function of channel size (D), in meter. The red bar shows the range of superfluid velocities inferred from the mass flow through the single nanohole. The open circles are previous results [16] with a temperature-dependent intrinsic critical velocity, whereas the crosses are temperature-independent (extrinsic) velocities. The straight line is the Feynman model of critical velocity.

symbols are dependent on channel size and follow more closely the Feynman critical velocity model $v_c = \frac{\hbar}{m_4 d} ln(\frac{d}{a_0})$, with a_0 the size of the vortex core [17]. Our data (red bar) are consistent with previous results for the intrinsic case.

In previous experiments, it was found that the critical velocity changes almost linearly with a decrease in temperature, and is well characterized by the equation $v_c = v_{c0}(1 - T/T_0)$ where T_0 and v_{c0} are fitting parameters. In Fig. 4, the data from Zimmermann *et al.* [9] are shown and compared to our normalized data for superfluid velocity. The parameter v_{c0} is the critical velocity extrapolation at $T = 0$ K and its value is typically of the order of 1 to 25 m/s [9,18]. For the nanohole flow, the extrapolation to $T = 0$ K yields values of v_{c0} from 8 to 45 m/s. The error on v_s becomes larger in the vicinity of T_λ because of the uncertainty on the superfluid density. This latter error prevents us from resolving the behavior of v_s very near T_λ. Nonetheless, the behavior of the superfluid velocity as a function of temperature in our nanohole is similar to that observed in larger channels, albeit the absolute values are the largest ever measured (to our knowledge) in a channel flow experiment.

Finally, we comment on the possibilities that are being opened up by this work. A theoretical model was constructed that takes into account the flow of liquid helium through the short pipe. This experiment demonstrates

de facto that mass flow measurements can be performed using liquid helium confined at the nanoscale. Our data are understood in terms of a two-fluid model modified for the specific geometry of the nanohole short pipe. As the size of the nanohole is reduced, and the transport becomes one dimensional, i.e., for $D \simeq 1$ nm and $L/D \gtrsim 10$, we expect new flow properties to emerge. In this 1D regime, a breakdown of the two-fluid model is likely to occur, giving way to the physics of Luttinger liquids which is predicted to form inside the nanopore [3].

*gervais@physics.mcgill.ca
[1] D. Krapf, M. Y. Wu, R. M. M. Smeets, H. W. Zandbergen, C. Dekker, and S. G. Lemay, Nano Lett. **6,** 105 (2006).
[2] J. Li, M. Gershow, D. Stein, E. Brandin, and J. A. Golovchenko, Nature Mater. **2,** 611 (2003).
[3] A. Del Maestro, M. Boninsegni, and I. Affleck, Phys. Rev. Lett. **106,** 105303 (2011), and references therein.
[4] G. M. Zassenhaus and J. D. Reppy, Phys. Rev. Lett. **83,** 4800 (1999).
[5] R. Toda *et al.*, Phys. Rev. Lett. **99,** 255301 (2007).
[6] J. Yoon, D. Sergatskov, J. Ma, N. Mulders, and M. H. W. Chan, Phys. Rev. Lett. **80,** 1461 (1998).
[7] J. Nyéki, R. Ray, B. Cowan, and J. Saunders, Phys. Rev. Lett. **81,** 152 (1998), and references therein.
[8] J. R. Clow and J. D. Reppy, Phys. Rev. Lett. **19,** 291 (1967).
[9] W. Zimmermann, Jr., C. A. Lindensmith, and J. A. Flaten, J. Low Temp. Phys. **110,** 497 (1998).
[10] Y. Sato, A. Joshi, and R. Packard, Phys. Rev. B **76,** 052505 (2007).
[11] E. Varoquaux and O. Avenel, Phys. Rev. B **68,** 054515 (2003).
[12] E. Varoquaux, M. W. Meisel, and O. Avenel, Phys. Rev. Lett. **57,** 2291 (1986), and references therein.
[13] M. Savard, C. Tremblay-Darveau, and G. Gervais, Phys. Rev. Lett. **103,** 104502 (2009).
[14] H. L. Langhaar, J. Appl. Mech. **9,** A55 (1942).
[15] J. M. Goodwin, Ph.D. thesis, University of Washington, 1968; J. S. Brooks and R. J. Donnelly, J. Phys. Chem. Ref. Data **6,** 51 (1977).
[16] E. Varoquaux, C.R. Physique **7,** 1101 (2006).
[17] The value of a_0 is ~1–6 Å but this uncertainty has a negligible effect on Fig. 4.
[18] W. Zimmermann, Jr., Contemp. Phys. **37,** 219 (1996).